4466 *Biochemistry* **2009,** *48,* 4466–4475
DOI:10.1021/bi802320q

BIOCHEMISTRY
including biophysical chemistry & molecular biology
Article

X-ray Structure of the High-Salt Form of the Peridinin-Chlorophyll *a*-Protein from the Dinoflagellate *Amphidinium carterae*: Modulation of the Spectral Properties of Pigments by the Protein Environment[†,‡]

Tim Schulte,[§] Frank P. Sharples,[∥] Roger G. Hiller,[∥] and Eckhard Hofmann*[,§]

[§]*Biophysics, Department of Biology and Biotechnology, Ruhr-University Bochum, D-44780 Bochum, Germany, and* [∥]*Biology Department, Faculty of Science, Macquarie University, NSW 2109, Australia*

Received December 19, 2008; Revised Manuscript Received April 16, 2009

ABSTRACT: Light-harvesting complexes have evolved into very different structures but fulfill the same function, efficient harvesting of solar energy. In these complexes, pigments are fine-tuned and properly arranged to gather incoming photons. In the photosynthetic dinoflagellate *Amphidinium carterae*, two variants of the soluble light-harvesting complex PCP have been found [main form PCP (MFPCP) and high-salt PCP (HSPCP)], which show small variations in their pigment arrangement and tuning mechanisms. This feature makes them ideal models for studying pigment−protein interactions. Here we present the X-ray structure of the monomeric HSPCP determined at 2.1 Å resolution and compare it to the structure of trimeric MFPCP. Despite the high degree of structural similarity (rmsd $C_\alpha-C_\alpha$ of 1.89 Å), the sequence variations lead to a changed overall pigment composition which includes the loss of two carotenoid molecules and a dramatic rearrangement of the chlorophyll phytol chains and of internal lipid molecules. On the basis of a detailed structural comparison, we favor a macrocycle geometry distortion of the chlorophylls rather than an electrostatic effect to explain energetic splitting of the chlorophyll *a* Q_y bands [Ilagan, R. P. (2006) *Biochemistry 45*, 14052−14063]. Our analysis supports their assignment of peridinin 611* as the single blue-shifted peridinin in HSPCP but also highlights another electrostatic feature due to glutamate 202 which could add to the observed binding site asymmetry of the 611*/621* peridinin pair.

Light harvesting is the first step in the photosynthetic process of conversion of light energy into chemical energy. The captured energy is used in the reaction centers (RCs)[1] to create a separated ion pair of chlorophylls (or bacteriochlorophylls) inducing a series of electron transfer reactions ultimately driving the reduction of CO_2 to carbohydrates. RCs are capable of absorbing light energy on their own, but without an antenna delivery system, the RCs would remain inactive most of the time (*2*). Thus, light-harvesting antennas increase the photosynthetic rate by increasing the effective absorption cross section and feeding the RCs with the gathered energy. In oxygen-evolving organisms, the RCs are located in the cores of the photosystems and are surrounded by diverse light-harvesting proteins which fall into two main groups: proteins with three membrane-spanning helices exemplified by the light-harvesting complexes (LHC) of higher plants and green algae and water-soluble phycobiliproteins characteristic of cyanobacteria, red algae, and cryptophytes. For both classes of light-harvesting antennas, extensive modification of the natural pigmentation has been found in different algal groups, thereby demonstrating the role of the antennas to extend the light absorption over a wide part of the visible spectrum (*3*, *4*). Outside basic LHCs and phycobiliproteins, some other remarkable light-harvesting proteins have evolved. One of the best studied examples is the peridinin-chlorophyll *a*-protein (PCP) characteristic of one group of photosynthetic dinoflagellates. PCP as a water-soluble antenna is located in the lumen of the chloroplast, thereby increasing the cross section around each photosystem by adding a third dimension (*3*). PCP has the highest carotenoid:chlorophyll ratio (4:1) of any light-harvesting protein, with the carotenoid dominating the absorption of the complex. The optical properties of peridinin [the molecular structure of peridinin (Per) is shown in Figure 1; the molecular structure of chlorophyll *a* (Chl-*a*) is given in Figure S1 of the Supporting Information] are characterized by a broad visible absorption band (see Figure 2) in the wavelength range between 400 and

[†]This work was supported by Sonderforschungsbereich 480 from the Deutsche Forschungsgemeinschaft (Teilprojekt C6) and by a grant from the Helmholtz Society in the framework of the Virtual Institute for Biological Structure Research (VH-VI-157) to E.H. and by a Macquarie University research development grant to R.G.H. T.S. acknowledges support by the Research School of the Ruhr-University Bochum.

[‡]Protein coordinates have been deposited in the Protein Data Bank (PDB) as entry 2C9E.

*To whom correspondence should be addressed: AG Proteinkristallographie, LS Biophysik, Gebäude ND04/316, D-44780 Bochum, Germany. Telephone: +49 (234) 3224463. Fax: +49 (234) 3214238. E-mail: Eckhard.hofmann@bph.rub.de.

[1]Abbreviations: Chl-*a*, chlorophyll *a*; CCG, conjugated carbonyl group; Dgd, digalactosyldiacylglycerol; HSPCP, high-salt PCP; ICT, intramolecular charge transfer state; LHC, light-harvesting complex; NCS, noncrystallographic symmetry; MFPCP, main form PCP; PCP, peridinin-chlorophyll *a*-protein; Per, peridinin; RC, reaction center; rmsd, root-mean-square deviation; vdW, van der Waals.

 Published on Web 4/16/2009

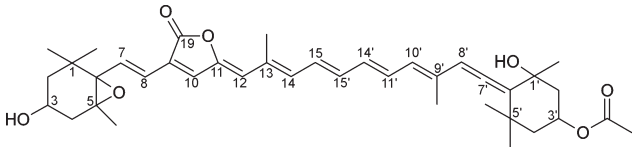

FIGURE 1: Structure of peridinin. Numbering according to IUPAC nomenclature.

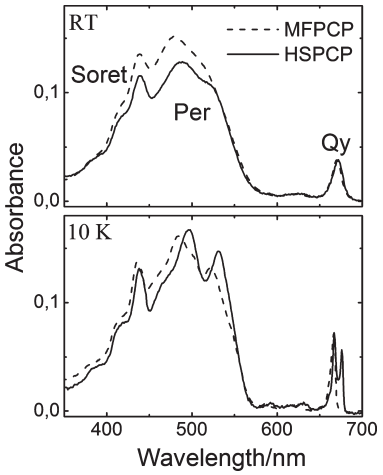

FIGURE 2: Absorption spectra of MFPCP and HSPCP measured at room temperature (RT) and at 10 K. Both spectra are normalized to the most prominent band in the Chl Q_y absorption region. The most prominent absorption bands are highlighted in the RT spectrum as follows: Soret (or B) bands of Chl-*a*; Q_y long wavelength absorption band of Chl-*a*; Per broad S_0-S_2 absorption. This figure was modified from Figure 2 of ref *20*.

550 nm, which represents a transition from the ground state, S_0, to the second excited singlet state, S_2. Absorption from S_0 to the lowest excited singlet, S_1, is symmetry forbidden in polyenes and carotenoids (*5*, *6*). After light absorption that promotes peridinin in the PCP complex into its S_2 state, the population of S_2 is depleted by energy transfer to Chl or by internal conversion to S_1 (*5*, *7*). It has been shown by ultrafast time-resolved optical spectroscopy (*8*) that the lifetime of the S_1 state of peridinin is strongly dependent on the polarity of the environment. These observations were explained by invoking the existence of an internal charge transfer state (ICT) that modulates the dynamics of the S_1 state perhaps as a means of controlling the transfer of energy to Chl (*8*−*11*). The exact nature of the ICT state is still a matter of debate (*5*, *7*), but its importance for the efficient energy transfer in PCP has been demonstrated, e.g., by Zigmantas and co-workers (*12*).

It is important to note that spectroscopic studies of peridinin (reviewed in ref *5*) form the basis for understanding energy transfer within the PCP complex, but a full understanding of how the system functions requires structural studies that reveal the architecture of the antenna system and the orientation of the pigments within the protein complex. Thus, revelation of the structural model of the main form of PCP (MFPCP) from the dinoflagellate *Amphidinium carterae* (*13*) was very important for our current knowledge of the energy transfer within PCP (reviewed in ref *7*).

Briefly, the protein with 313 amino acids consists of two pseudosymmetrical α-helical domains. Each of these encloses an internal pigment cluster of four peridinins (Pers) arranged in van der Waals (vdW) contact around a central chlorophyll *a* (Chl-*a*) macrocycle. In some species of dinoflagellates [*Heterocapsa pygmaae* (*14*) and *Symbiodinium muscatinei* (*15*)], the PCP has an apoprotein of 140 amino acids but the pigmented native PCP is a homodimer. Although the data are limited, the pigment composition and CD and visible spectra of dimeric PCPs closely resemble those of *A. carterae* (*16*, *17*).

This conserved domain arrangement of PCP complexes is reflected in their spectroscopic features. Simplified, each of the two pigment clusters works as an independent harvesting system (model depicted in ref *18*) but can transfer energy between the chlorophylls by the Förster mechanism (*19*−*23*). In each cluster, excitation develops as follows: after excitation the energy is shared by the four peridinins via their S_2 excited states (*18*), a small amount of this energy being directly transferred to the Chl-*a* Q_x state (*12*, *24*, *25*). The majority of the energy is transferred via the S1/ICT state to the Chl-*a* Q_y state (*26*, *27*), but only by three of the four peridinins per cluster (*18*). The one not transferring via S_1 has been proposed to be blue-shifted in energy and has been assigned to Per-612[2] (*18*). The energy shift has been explained by a conformational distortion of Per-612 within the structure as compared to the other peridinins (*28*).

To test this assumption, work has been focused on the only other reported variation in the type of PCP, the high-salt PCP form (HSPCP) from *A. carterae*, so named because it elutes from a cation exchange column at much higher NaCl concentrations than MFPCP (*29*). The HSPCP apoprotein is composed of 324 amino acids compared to 313 for MFPCP, but the level of sequence identity is only 31%. Intriguingly, HSPCP differs from MFPCP in having six Per molecules per two Chl-*a* molecules compared to eight Per molecules per two Chl-*a* molecules in MFPCP. As energy transfer efficiency seems not to be affected by this loss (*20*), either the two missing peridinins are less important for the direct energy transfer to Chl-*a*, or the remaining Pers are more efficiently coupled to the Chls. Ilagan and co-workers have investigated the differences in these complexes by using steady-state (see Figure 2) and femtosecond time-resolved optical methods combined with quantum chemical computations on the basis of a structural model of HSPCP from our group (*30*). As dominant spectroscopic features of HSPCP, they observed the loss of the two blue-shifted peridinins 612 and 622 from MFPCP, the existence of another blue-shifted peridinin, and an energetic splitting of the chlorophylls in the two domains when measured at 10 K (see Figure 2). Ilagan and co-workers favor electrostatic effects of key residues as the main cause of the shift of a peridinin to the blue as well as splitting of the chlorophyll Q_y band. Protein sequence variations can, however, induce differences in more property levels than in electrostatics. These levels can include changes in (i) the overall protein scaffold, (ii) single residues in terms of polarity, charge (electrostatics), or H-bonds, (iii) pigment geometry distortions, and (iv) pigment−pigment interactions.

Our detailed structural analysis of the refined HSPCP structure reveals remarkable differences of the pigment binding sites at the level of pigment geometry distortions and at the level of single residues. Taking into account the spectroscopic and computational results of Ilagan and co-workers (*30*), we propose a different mechanism for the splitting of the chlorophyll Q_y bands and expand the electrostatic explanation to account for the blue-shifted peridinin.

[2]For the sake of clarity, we align the pigment numbering for HSPCP (2C9E) with that of the structural model of MFPCP (1PPR): Chl-1327 = Chl-601*, Chl-1328 = Chl-602*, Per-1329 = Per-611*, Per-1330 = Per-613*, Per-1331 = Per-614*, Per-1333 = Per-621*, Per-1334 = Per-623*, Per-1335 = Per-624*, Dgd-1332 = Dgd-615*, and Dgd-1336 = Dgd-625*.

EXPERIMENTAL PROCEDURES

Protein Expression and Purification. High-salt PCP was prepared as described previously (*29*). Briefly, *A. carterae* was cultured at low light intensity (20 μmol m^{-2} s^{-1}) in Provasolis enriched seawater. Cells were harvested by flocculation using 0.5 mM $AlK(SO_4)_2 \cdot 12H_2O$. Following a wash using 50 mM Tricine and 20 mM KCl (pH 7.5), cells were broken by a single passage through a French pressure cell operated at 80 MPa. The brick red supernatant after centrifugation contained mainly PCP complexes, of which ~2% were of the high-salt form. We do not know whether this low proportion of HSPCP can be increased by altering the growth conditions. PCPs were further purified by ammonium sulfate fractionation between 70 and 90% concentration followed by dialysis against 5 mM sodium acetate (pH 5.0). Separation of MFPCP and HSPCP was achieved by cation exchange chromatography using a CM Tris-acryl column with a linear NaCl gradient. HSPCP eluted well separated from MFPCP at ~250 mM NaCl. Purified protein was dialyzed against 50 mM Tricine, 20 mM KCl, and NaN_3 (pH 7.5) and stored at −20 °C until use.

Crystallization and Data Collection. Because of the low yield of HSPCP, protein from several purification rounds was used for crystallization trials. After thawing, protein was concentrated using a centriprep spin concentrator with a molecular mass cutoff of 10 kDa. The protein was centrifuged for 30 min at 17000*g* to remove aggregates formed during the buffer exchange and concentration procedure. The resulting protein concentration of ~1 mg/mL was determined spectroscopically. After the sample had been screened with the Crystal Screen Cryo (HamptonResearch, Aliso Viejo, CA) at 18 °C via the sitting drop method, several adnate thin needles and plate crystals were obtained in condition 41 [5% 2-propanol, 85 mM HEPES (pH 7.5), 17% PEG 4000, and 15% glycerol]. After mechanical separation, we were able to mount and shock-freeze a single crystal in liquid nitrogen. Diffraction data were collected to 2.1 Å resolution at 100 K at the ESRF (Grenoble, France) on beamline ID14-EH4. The data were processed and scaled using programs from the XDS package (*31*). Data statistics are listed in Table 1.

Structure Determination and Refinement. The HSPCP structure was determined by molecular replacement using MOLREP (*32*) as implemented in CCP4 (*33*). Monomer M of the MFPCP trimer (PDB 1PPR) was selected as a search model, including pigment and lipid molecules. MOLREP yielded two possible solutions well separated from the rest with correlation coefficients of 0.197 and 0.191 (the closest following three solutions had correlation coefficient values of ~0.155). The two best solutions correspond to a pseudo-2-fold symmetry of the PCP structure. The top solution was chosen for refinement in CNS (*34*). Rigid body refinement, simulated annealing, and conjugate gradient procedures without manual modification of the model resulted in an R_{cryst} of 39% and an R_{free} (5% of data randomly assigned) of 45.4%. The model was improved by alternating refinement in CNS and model building in Coot (*35*) using prime-and-switch improved maps to reduce model bias (*36*). Due to the absence of electron density, two peridinins (Per-612 and Per-622), the phytol tails of the chlorophylls, and both lipids were removed from the model in this initial stage. The pseudo-2-fold symmetry was used both for averaging of maps and for noncrystallographic symmetry (NCS) restraints during refinement. After crucial residues in both amino-terminal (N-terminal) and carboxy-terminal (C-terminal) domains had been examined, the model was rotated by 180° around its pseudo-2-fold axis. During the subsequent refinement, NCS restraints were partially released where appropriate. The phytol tails and both lipids could be replaced into the calculated electron density map. Peridinins were fitted using topology and parameter data produced with PRODRG (*37*). Topology and parameter data for chlorophyll *a* and digalactosyldiacylglycerol were taken from ref *13*. Repeated rebuilding (using $3mF_o - 2DF_c$ and $mF_o - DF_c$ maps) and refinement of the structure (including two chlorophylls, six peridinins, two digalactosyldiacylglycerols, and an additional metal ion) reduced the R_{cryst} to 17.4% (R_{free} = 21.9%). Statistics for the final structure refinement are given in Table 1. The coordinates have been deposited in the PDB as entry 2C9E.

The chlorophyll and peridinin omit maps shown in Figure 6B and Figure S4 of the Supporting Information were calculated as follows: (1a) removal of both Chls and the His-coordinated water molecules from the model, (1b) removal of each single peridinin, (2) coordinate perturbation of the whole model by an average of 0.5 Å using Moleman2 (*38*), and (3) calculation of $3mF_o - 2DF_c$

Table 1: Summary of Data Collection and Structure Refinement Statistics[a]

Data Collection	
space group	*P*2(1)
unit cell parameters	*a* = 46.58 Å, *b* = 62.67 Å, *c* = 63.35 Å α = 90°, *β* = 100.89°, *γ* = 90°
X-ray source	ESRF beamline ID14-4
temperature (K)	100
resolution limits (Å)	37−2.1 (2.25−2.1)
wavelength (Å)	0.9198
no. of observations	66197 (8017)
no. of unique reflections	20528 (3425)
redundancy	3.2 (2.3)
completeness (%)	97.5 (87.6)
I/σ	9.9 (3.8)
R_{sym} (%)	10.8 (37)
R_{meas} (%)	10.1 (31.5)
$R_{mrgd\text{-}F}$ (%)	10.8 (37)
Structure Refinement	
PDB entry	2C9E
R_{cryst} (%)	17
R_{free} (%)	22
no. of protein atoms	2360
no. of solvent atoms	289
no. of heterogeneous atoms	539
mean isotropic *B* value (Å^2)	28.6
protein main chain atoms (N−CA−C−O) (Å^2)	27
solvent (Å^2)	39.4
peridinins (Å^2)	22.5
chlorophylls (Å^2)	20
lipid (Å^2)	29.6
rmsd for ideal bond lengths (Å)	0.017
rmsd for ideal bond angles (deg)	2.1
Molprobity[b]	
Ramachandran	
favored (%)	98.7
allowed (%)	100
all atom clash score (percentile)	3.45 (99th)
Molprobity score (percentile)	1.75 (92nd)

[a] Data in parentheses represent values in the highest-resolution bin. [b] From ref *64*.

maps using CNS (*34*) refinement applying simulated annealing at 3000 K. Calculations of surface accessible areas and contact tables were performed using WHAT IF (*39*). All figures illustrating the structures were created with Pymol (*40*).

RESULTS AND DISCUSSION

Overall Structure. The overall structure of HSPCP is shown in Figure 3A. The protein folds into 17 α-helices with short linker regions, which form the scaffold for the bound cofactors. The arrangement can be described by analogy to a ship as was done for the main form PCP structural model (*13*). The bow, sides, stern, and deck of the ship are formed by the protein helices, and the space formed inside resembling the freight room contains the pigments and lipids as cargo. N- and C-terminal domains of the protein form independent folding domains, which are related by a pseudo-2-fold symmetry (Figure 3A,B). A long connection between both domains forms the keel of the ship. Each domain binds a pigment cluster consisting of one chlorophyll *a* molecule, three peridinin molecules, and one molecule of the thylakoid lipid digalactosyldiacylglycerol (Dgd). The cofactors again obey the pseudo-2-fold symmetry. The overall topology is shown in Figure 3B with the helices arranged in a pairwise fashion resembling the Greek key topology also found for the MFPCP structure (*13*). N- and C-terminal domains superpose very well spatially with an rmsd of 0.72 Å [152 C_α atoms aligned, calculated with CCP4 mg SSM superimpose (*41*)] even though the level of sequence identity is only 50% (*29*) (sequence alignment shown in Figure S2 of the Supporting Information).

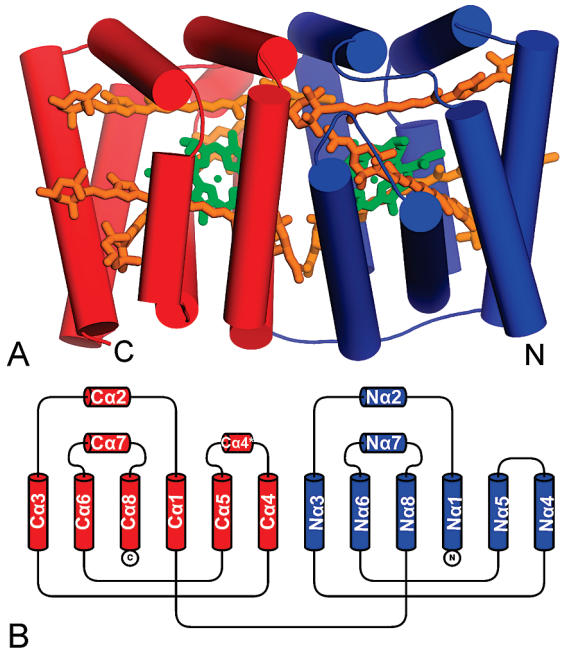

FIGURE 3: (A) View of the HSPCP structural model. The protein helices are shown as cylinders connected by loops. The N-terminal domain is colored blue and the C-terminal domain red. Per is represented as an orange stick and the Chl porphyrin ring as a green stick. The lipid Dgd and the Chl phytol tail have been omitted for better illustration. (B) Topology diagram of HSPCP (N-domain, blue; C-domain, red).

The refined model consists of the apoprotein and two Chl-*a*, six Per, and two Dgd molecules. Residues 165−173, which are part of the linker region between N- and C-terminal domains, have been omitted due to missing density. This observed disorder could be a result of proteolytic degradation in the keel region as cleavage at Arg-170 has been observed after prolonged storage (*29*). Because of the lack of a sufficient number of crystals, we were not able to address this question by analytical methods, i.e., mass spectrometry. In the crystal, no strong interactions between neighboring monomers are observed, arguing against a higher oligomeric state of HSPCP being biologically relevant.

Comparison with MFPCP Protein. The structure of HSPCP can be best described in comparison to the structural model of MFPCP. The differences between the two PCP forms have been analyzed in detail (*20*, *29*, *30*, *42*) using spectroscopic as well as biochemical methods. Here the two structural models are compared on the level of the protein scaffold, pigment composition, and interaction between the pigments and their binding environment.

(i) Protein Scaffold. The protein backbones superpose surprisingly well [Figure 4; rmsd of 1.89 Å for 286 aligned C_α atoms calculated with CCP4 mg SSM superimpose (*41*)] given the rather low level of sequence conservation (31%) and the loss of two integral carotenoid molecules. Major structural deviations are observed only in the regions which are adapted for trimerization in the case of MFPCP, something which is not needed for the monomeric HSPCP. These major structural deviations include the elongation of the helices on the deck of the protein ship (see Figure 4, especially helices Nα2 and Cα2). Overall, in HSPCP the two protein domains are moved apart to some extent (visible in the superposition in Figure 4) which results in a larger distance between the Chl-*a* molecules in HSPCP than in MFPCP (Figure S3B of the Supporting Information). The space inside the protein scaffold for the cofactors is slightly increased from 22870 $Å^3$ in the case of MFPCP to 23660 $Å^3$ in HSPCP [calculated with Voidoo (*43*)].

Structural motifs on the secondary structure level, in particular α-helices, are capable of inducing large spectral shifts of

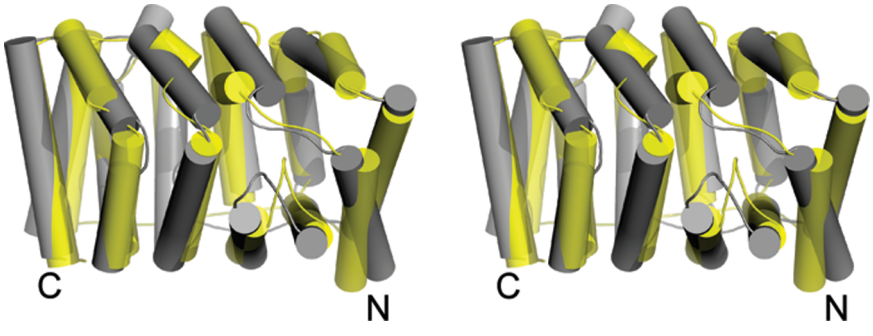

FIGURE 4: Superimposition of the protein helices of HSPCP (gray) and MFPCP (yellow) in stereoview. View tilted by ~20° compared to Figure 3A.

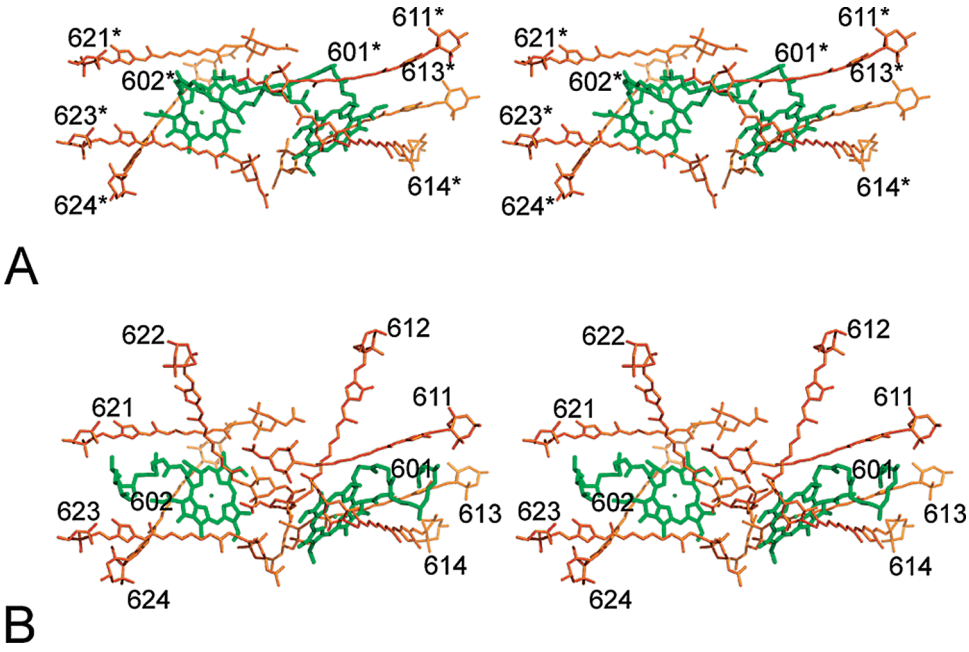

FIGURE 5: Comparison of HSPCP (A) and MFPCP (B) pigment arrangement in stereo representation. Per and Chl are colored orange and green, respectively. The orientation is similar to that in Figure 1A.

pigments, which has been demonstrated in the case of bacteriochlorophylls in the FMO protein (*44*), but the very similar overall positioning of helices in HSPCP and MFPCP (Figure 4) suggests it will not contribute significantly to different chromophore tuning in the complexes. Additionally, the two domains of PCP are related by a pseudo-2-fold symmetrical axis. Therefore, the effects of the helices should be similar in both domains and cannot be the major reason for the observed asymmetry in the optical properties of the two pigment clusters in HSPCP.

(ii) Pigment Composition. The pigments are arranged in a manner similar to that in MFPCP (*13*) (for a comparison, see Figure 5 and Figure S3 of the Supporting Information), but two main changes are obvious. The first is that the two peridinins 612 and 622 of MFPCP are missing in the HSPCP structural model. This is consistent with earlier conclusions based on spectroscopic and computational data (*18*, *20*, *29*). Loss of these peridinins is less dramatic for energy transfer efficiency within the pigment cluster as they are proposed not to be involved in the direct energy transfer to the chlorophyll molecule (*18*).

The second remarkable difference is the chlorophyll positioning. In HSPCP, the chlorophyll phytol tails are rearranged to fill the free space of the missing peridinins. In addition, we observe a small tilt of the macrocycle of ~3° (see Figure S3B of the Supporting Information) and an increased Chl-*a*−Chl-*a* center distance, from 17.4 Å in MFPCP to 18.4 Å in HSPCP.

Energy transfer between the two chlorophylls within the PCP complex is best described applying the Förster energy transfer mechanism (*19*−*23*). In Förster theory, the energy transfer rate depends on the distance, the orientation, and the spectral overlap of the pigments (*45*). Spectroscopic analysis of both complexes using time-resolved absorption spectroscopy has revealed that energy transfer in HSPCP is 4.2 times slower than in MFPCP (*30*). Förster theory calculations with our structural data on HSPCP by Ilagan and co-workers have shown that the differences in the distance and the orientation can account for an only 30% rate loss in HSPCP. Another fraction of ~12−48% of energy transfer rate loss can be explained by changes in the spectral overlap of the two chlorophylls in HSPCP. Unlike the chlorophylls in MFPCP, the chlorophylls in HSPCP are energetically not equal but show a splitting of the Q_y absorption peak at cryogenic temperature (see Figure 2) (*20*, *30*). This observation of different chlorophyll site energies will be discussed in detail in the next section.

The remaining fraction of rate loss might be explained by the absence of the two peridinins 612 and 622 which could act as bridging polarizable units enhancing the energy transfer rate in MFPCP (*30*). This bridging cannot be accomplished by the phytol tails occupying the space of Per-612 and Per-622 as the tails do not contain delocalized electrons in the form of a π-conjugated system.

(iii) Pigment Binding Sites within HSPCP. (a) Chlorophyll Binding Sites. The chlorophylls in HSPCP are bound in the same way that has been described for MFPCP (*13*) despite a different orientation of their phytol tails. The central magnesium atom of Chl-*a* is coordinated via a water molecule occupying the fifth coordination site. This water molecule is in turn coordinated by a conserved histidine residue. No other polar contacts with the tetrapyrrole rings of the chlorophylls are found in the HSPCP structure. Therefore, the chlorophyll environment is mainly generated by the peridinins, the lipid fatty acid chains, and apolar or aromatic residues.

(b) Interpigment Coupling Effects. The observed chlorophyll Q_y energy splitting can have different molecular origins: wavelength shifts can be generated by the protein environment (local effects like H-bonds, close charges; protein-induced conformational flexibility of the chromophore; charges induced by secondary structural elements) and by pigment−pigment interactions (excitonic coupling) (*44*, *46*−*49*). In the case of PCP, interdomain chlorophyll coupling is assumed not to play a role because the separation is too large and the orientation factor very small. Exciton coupling between the Chl-*a* molecules in MFPCP was measured to be in the range of ~10 cm^{-1} (*19*). Differences in peridinin−chlorophyll interaction are not very likely to cause energetic shifts of the chlorophyll since loss of the blue-shifted peridinin (Per-612/Per-622) affects both domains similarly. In addition, these blue-shifted peridinins interact only

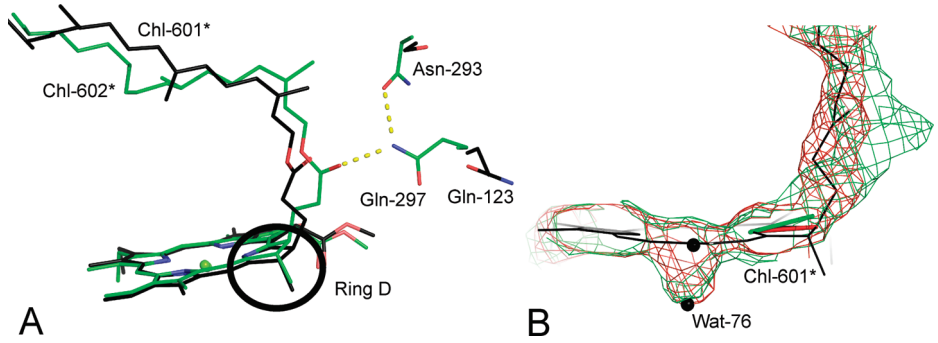

FIGURE 6: (A) Chlorophyll coordination in the N-domain and C-domain (black and green, respectively) . (B) Superimposition [done with Chimera (*65*)] of slices through chlorophyll omit electron density maps (contoured at 3σ) of Chl-601* (red) and Chl-602* (green). The model of Chl-601* is colored black. The green and red bars indicate connections between the N_{24} and C_{17} atoms (for atom numbering, see Figure S1) of Chl-601* (red bar) and Chl-602* (green bar) to illustrate the ring puckering of Chl-602*.

weakly with the chlorophyll Bx states (*17*). Per-614 in MFPCP is supposed to show the strongest interaction with Chl-*a* being the primary triplet energy quencher (*42*, *50*, *51*). Per-614 also shows coupling interaction with Chl-*a* in step scan FTIR experiments (*52*) as well as in transient absorption measurements (*53*). However, neither our structural comparison nor quantum mechanical calculations (*30*) point to Per-614 and Per-624 being energetically unique and distinct from the other peridinins or each other.

(c) Chlorophyll Binding Geometry. In summary, pigment−pigment interactions are not very likely to induce the observed energetic splitting of the chlorophylls. What remains are changes induced by a different binding environment. The MNDO-PSCDI calculations on the HSPCP complex (including all charged residues within 8 Å) were able to reproduce the observed splitting (*30*). Two positively charged residues were identified as the key factors for this effect, but in both cases, the charged functional groups are surface-exposed and more than 12 Å from the π-conjugated systems of the chlorophylls. Therefore, we favor another structural difference between both binding sites as the major source for the splitting. In the C-domain of HSPCP, the carbonyl oxygen of the phytol tail ester is in the proximity of the amino group of Gln-297 and able to build up a hydrogen bond {0−1GF = 0.626 [0−1 geometry factor calculated with WHAT IF, 0 = no hydrogen bond, 1 = optimal hydrogen bond (*39*)]} (Figure 6A). This positioning of Gln-297 is stabilized by an additional hydrogen bond to Asn-293 (0−1GF = 0.576). The fixation of the carbonyl oxygen leads to a reorientation of the phytol tail which is clearly present in the superimposition of chlorophyll omit electron density maps (see Figure 6B). This in turn leads to an out-of-plane deformation of ring D in the Chl-602* molecular model compared to the Chl-601* model. The resulting displacement of the corresponding C-17 atoms of ring D (Figure 6A,B; Chl atom numbering given in Figure S1 of the Supporting Information) of the superimposed chlorophylls is approximately 0.4 Å and is therefore larger than the estimated distance uncertainty of 0.3 Å based on the positional error of the model.[3] In the MNDO-PSCDI calculations of Ilagan and co-workers, the chlorophylls were taken without the phytol tails to accelerate the calculations. Thus, the influence of a reorientation of the phytol tail toward a possible ring deformation was impossible to detect. It is known that protein-induced deformation of the porphyrin macrocycle can account for spectral wavelength shifts to the red of up to several tens of nanometers (*54*, *55*). Indeed, a preliminary MNDO-PSDCI calculation of the two isolated chlorophylls using the fixed crystallographic positions of the heavy atoms (and therefore maintaining the ring deformations) gave clear indications for a significant energetic shift for one of the two chlorophylls (R. Birge, personal communications). Therefore, this structural mechanism seems to be sufficient to explain the experimental observation of a splitting of the Q_y absorption band at low temperatures in HSPCP. Future calculations should check whether the fixation of the phytol tail by the observed hydrogen bonds is real and leads to the observed energetic shift of Chl-602*. The influence of the hydrogen bond to the carbonyl itself can be neglected as it is not directly attached to the π-conjugated system of the porphyrin ring.

(d) Peridinin Binding Sites. The peridinins are arranged around the chlorophyll molecule in such a way that individually most of their surface is covered by the other bound cofactors. The rest of the surface of the polyene chain is occupied by aromatic and apolar side chains, whereas the polar head groups protruding from the protein interior are coordinated by polar and charged amino acids and solvent.

Despite the very similar individual peridinin binding sites found in MFPCP and HSPCP, spectroscopic analysis shows spectral heterogeneity of the peridinins in both complexes (*17*, *20*, *28*, *56*). Within MFPCP, four spectrally distinct peridinins have been found, one of them located at a higher energy level and therefore blue-shifted in the absorption spectrum. Computational analysis has pointed toward Per-612 being the blue-shifted peridinin and not transferring energy to Chl-*a* as efficiently as the other three peridinin molecules (*17*, *18*).

(e) Geometry of the Peridinins. The higher energy of Per-612 has been attributed to a distorted geometry due to its binding site (*28*). MNDO-PSCDI calculations have shown that Per-612 has inverted S_1-S_2 energy levels, and the authors claim that Per-612 increases the extent of energy transfer to the other peridinins by increasing S_2-like state populations. Despite the observation that the two putative blue-shifted peridinins are missing in HSPCP, Ilagan and co-workers found that one blue-shifted peridinin is still necessary to simulate the 10 K absorption spectrum of the HSPCP complex (*20*, *30*).

[3]We estimate the overall positional error of the HSPCP model to be around 0.2 Å [Luzzati plot = 0.215 Å, estimated maximal error = 0.126 Å, DPI = 0.183 Å; calculated with SFcheck (*1*)]. While it is difficult to use these global indicators for individual atoms, we expect similar values for the atoms of interest. The positional uncertainty in the protein core will generally be substantially smaller (as seen in lower *B* values), but this might be counterbalanced by a higher error due to the use of individual sets of geometric restraints for the cofactors in refinement.

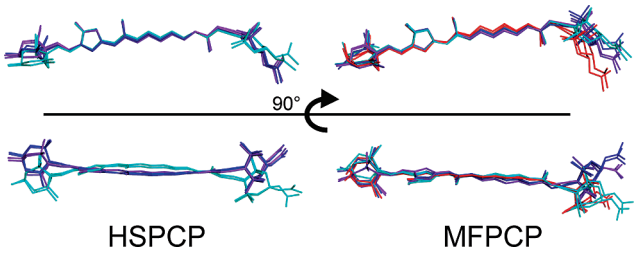

FIGURE 7: Superimposed peridinins within HSPCP and MFPCP in two different views: Per-611 and Per-621, cyan; Per-612 and Per-622, red; Per-613 and Per-623, blue; and Per-614 and Per-624, purple.

The superimposed peridinin molecules within each complex are shown in Figure 7, in two different orientations. In MFPCP, Per-612 and Per-622 exhibit a varied distortion at the allene end of the molecule which is not present in any of the HSPCP peridinins. Overlay of the HSPCP peridinins clearly indicates that Per-611* and Per-621* are bent in the opposite direction compared to the other peridinins, which is also observed in peridinin omit electron density difference maps (Figure S4 of the Supporting Information). This different bending of the peridinin molecules is not observed in MFPCP. In general, peridinins in HSPCP are bent to a higher extent, but the pairs from the two domains superpose well, excluding peridinin geometry as a contributor to the observed symmetry breaking of a single peridinin.

(f) Electrostatics of the Peridinin Binding Environments. Charge substituting mutations could induce electrostatic differences and thereby cause different peridinin site energies. The pseudo-2-fold symmetry (see Figure 3) of the PCP complexes allows comparison of a peridinin in one domain with its mate in the other. The blue-shifted peridinin should reveal itself as being located in another binding site compared to its mate. The sequence alignment of the two HSPCP domains (Figure S2 of the Supporting Information) indicates 33 mutations involving a charge substitution. Only six residues within these 33 mutations have their putatively charged functional groups (carboxy group of Glu and Asp, guanidino group of Arg, and ammonium group of Lys) within ~8 Å of the π-conjugated system of a peridinin molecule (WHAT IF was used to make a contact list; The allowed distance between vdW surfaces of two atoms was set to 5 Å). Their location with respect to their corresponding peridinin molecules is shown in Figure 8 for each peridinin pair. All substitutions creating positive charges are located at the epoxy end of the peridinin molecules. In contrast, the negative charges of Glu-136 and Glu-202 are located at different sites with respect to Per-611* and Per-621*. Both are not matched by similar charges in the other respective domain. This clearly indicates an asymmetry in the coordination sites of the two peridinin molecules. However, from this simple analysis alone, we are not able to tell which of the two peridinins is energetically different.

In MNDO-PSCDI calculations with our HSPCP structural model, Per-611* was found to be blue-shifted with respect to all other peridinins in the complex (*30*). The negative charge of Glu-136 was held responsible for the observed shift by repulsing the electronic charge movement during excitation of the peridinin molecule. In this interpretation, all peridinins within HSPCP are initially assumed to be located in binding environments with similar site energies. Placement of the negatively charged Glu-136 modifies selectively the site energy for Per-611*, which is then observed as a blue-shifted peridinin. However, Ilagan and co-workers have not discovered the unique

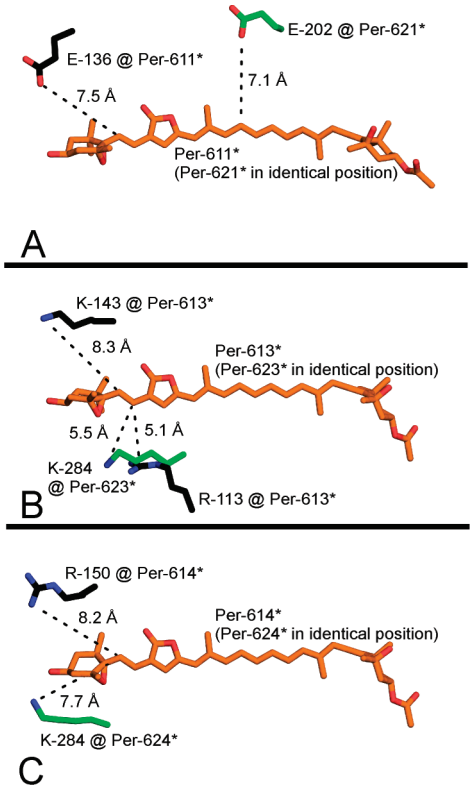

FIGURE 8: Schematic view showing the position of the six charge substituting residues with respect to their corresponding peridinins. For each peridinin symmetry pair [(A) Per-611* and Per-621*, (B) Per-613* and Per-623*, and (C) Per-614* and Per-624*], only the peridinin in the amino-terminal domain (Per-61*x**) is shown. Residues belonging to the Per-61*x** binding sites are colored black, and residues belonging to the Per-62*x** binding sites are colored green. The closest distances of the charged functional groups to the Per π-conjugated system are indicated by a dashed line.

position of Glu-202 in their analysis and therefore have not discussed its role as a possible factor for the observed peridinin site energy shift.

An alternative explanation for the observed blue shift of Per-611* could be that the peridinin pair of 611* and 621* is located in a binding environment with a higher site energy (therefore blue-shifted). Despite our assumption that the observed peridinin geometry differences (discussed in the previous section) between the peridinin pair of Per-611* and Per-621* and the other peridinins cannot account for a single peridinin to be shifted to higher energies, the opposite bending could increase the site energies of both Per-611* and Per-621*.

Then, placement of the negatively charged Glu-202 could selectively lower the site energy for Per-621*, thereby rendering it comparable to the remaining peridinin sites. It is worth noting that both residues, Glu-136 and Glu-202, could be contributing to the observed splitting of the two peridinins.

Furthermore, effects of the local environment on the effective charges of side chains should be considered. In contrast to the position of Glu-136 discussed above, the side chain of Glu-202 is not as accessible to the solvent [surface accessible area of side chain carboxy group Glu-136 (12 Å^2) and Glu-202 (6 Å^2); calculated with WHAT IF], making it less susceptible to counterions from the solvent. Its higher inaccessibility value and its unique location within the peridinin binding site make Glu-202 a more appropiate candidate than Glu-136 to cause a shift of a peridinin site energy. Although in MFPCP some

asymmetries are present (Per-613 and Per-624), such a combination of relative inaccessibility and a unique location of a single residue is not present (compare Peridinin-Distance-Plots of HSPCP and MFPCP in Figures S5 and S6 of the Supporting Information and accessibility values in Table S1 of the Supporting Information). In fact, Glu-202 in HSPCP is the only residue of all relevant charge substituting residues (in HSPCP and MFPCP) which is classified as buried by the Propka 2.0 server (*57*) (see Table S1). Its pK_a value is calculated to be around 4, meaning that almost all Glu-202 residues within a HSPCP sample are deprotonated at pH 7.5 [pH of the buffer taken via spectroscopic measurements (*20*, *30*)].

In addition to the electrostatic effects described above, a further red shift of Per-621* could be caused by a water cluster which is close to Glu-202 and reaches the π-conjugated system of Per-621* [crystallographic waters placed into a cavity shown in Figure S7 of the Supporting Information; cavities in HSPCP analyzed with Voidoo (*43*); cavity mesh generated with Caver (*58*)]. Peridinin absorption is known to shift to a lower energy with an increase in polarizability (*8*, *28*), and placement of water molecules leads to a red shift of peridinin in MNDO-PSCDI calculations (*28*). Thus, the water cluster would add to the electrostatic energetic splitting mechanism between Per-611* and Per-621*.

Ideally, we would like to test these hypotheses experimentally by using site-directed mutagenesis. As this is currently not possible for HSPCP, the role of Glu-136 in tuning the site energy of Per-611* has been tested using the in vitro reconstitution system of N-MFPCP (RFPCP) (introduced in ref *59*). In MFPCP, Glu-133 is in the same position as Glu-136 in HSPCP (see the sequence alignment in Figure S2 of the Supporting Information), but its negative charge is compensated by an adjacent positively charged lysine (see in Figure S8 of the Supporting Information). Mutations of these residues using RFPCP did not produce significant differences in absorption spectra at either room temperature or 10 K (T. Schulte et al., unpublished results), calling into question the role of Glu-136 as the major factor involved in the observed spectral tuning.

(g) Hydrogen Bonding to the Peridinins. The spectroscopic features of peridinin particularly depend on its conjugated carbonyl group (CCG) (*5*, *7*). Thus, another relevant consideration is hydrogen bonding to the carbonyl oxygen of the π-conjugated lactone group. Experiments with peridinin in solvents differing in polarity and ability to form hydrogen bonds show that hydrogen bonds to the CCG stabilize a red form of peridinin (*60*). Hydrogen bonds to CCGs of astaxanthin in α-crustacyanin are discussed as being involved in the bathochromic shift of the carotenoid (*61*, *46*). In HSPCP, several hydrogen bonds to the CCGs of peridinins are observed. The CCG of Per-623* (Figure S9 of the Supporting Information) is hydrogen bonded by a hydroxyl group of the lipid Dgd, whereas no hydrogen bond is observed in the case of the symmetry-related Per-613*. Interestingly, the CCGs of the equivalent peridinins in MFPCP (623 and 613) are symmetrically hydrogen bonded via water molecules. Again, this could be indicative of the loss of a red-shifting factor causing the observed blue shift of a single peridinin. In HSPCP, we also observe symmetrical hydrogen bonds to the CCGs for Per-611* and Per-621* with the amino group hydrogens of Asn-130 (0−1GF = 0.627) and Asn-304 (0−1GF = 0.714).

Another functional group of peridinin is the oxacyclopropane ring which is separated from the π-conjugated system by a single bond. The influence of a hydrogen bond on the epoxy group of peridinin in terms of spectral tuning has not been discussed so far. The oxygen of the oxacyclopropane ring of Per-611* is coordinated by the amino group of Gln-123 (0−1GF = 0.576) (Figure S10 of the Supporting Information), whereas the ring of Per-621* is not coordinated by the corresponding residue, Gln-297. Although the observed hydrogen bond might not have a direct influence, there could be a secondary effect resulting from different orientations of the two glutamine residues. Different orientations of polar groups with respect to the dipole moment of a chromophore can cause spectral shifts, i.e., of retinal in rhodopsin (*62*, *63*).

CONCLUSION

The overall folding of the monomeric HSPCP crystal structure is highly homologous to that of each monomer of the trimeric MFPCP structural model, despite a rather low level of sequence identity. Both complexes consist of two separate domains related by a pseudo-2-fold symmetry each containing a separate pigment cluster.

The most obvious difference between the two PCP complexes is the loss of the two peridinins 612 and 622 which was proposed earlier by spectral analysis. Additionally, the phytol chains of the chlorophylls and the two conserved lipid molecules are rearranged dramatically, filling the space left by the missing peridinins. This rearrangement leads to an asymmetric coordination of the phytol tails in the two domains which causes a deformation of one of the chlorophyll macrocycles. This deformation could explain the observed chlorophyll splitting in low-temperature absorption spectra of HSPCP, instead of an electrostatic effect proposed in recent calculations by Ilagan and co-workers.

Another remarkable feature of HSPCP is the occurrence of another blue-shifted peridinin, although the presumably blue-shifted peridinin pair (Per-612 and Per-622) from MFPCP is absent in HSPCP. Our structural data suggest several possible mechanisms for this tuning, clearly illustrating the complex cooperation of structural factors in this process. We could observe differences in pigment conformation, electrostatic interactions, and hydrogen bonding patterns, all possible players in the tuning process. These differences mainly point to the peridinin pair of 611* and 621* as being located in different binding sites. Ilagan and co-workers have highlighted the electrostatic influence of E-136 on Per-611*; we want to add the influence of E-202 on its mate Per-621*. The negative charge of E-202 in combination with its unique location with respect to the peridinin π-conjugated system contributes to the peridinin pair asymmetry.

A conclusive description of the protein effects demands more detailed computational investigations. On the basis of our data, these have to include all additional cofactors, namely, the lipids, internal water molecules, and the effect of counterions. The possibility of selectively "switching off" charged residues will allow the conclusive assignment of the individual amino acids toward the tuning.

ACKNOWLEDGMENT

We thank Dr. Harry Frank for providing the spectral data to create Figure 2 and Dr. Robert Birge for testing our assumptions about the chlorophyll ring puckering and for giving insights into unpublished results. Finally, we thank Drs. Tomáš Polívka, Harry Frank, and Robert Birge for critically reading the manuscript and for stimulating discussions. We thank the beamline

staff at ID14-4 at the European Synchrotron Radiation Facility for assistance during data collection. We also thank Dr. Dean Madden for his support in the early stages of the project.

SUPPORTING INFORMATION AVAILABLE

Ten figures and one table. This material is available free of charge via the Internet at http://pubs.acs.org.

REFERENCES

1. Vaguine, A. A., Richelle, J., and Wodak, S. J. (1999) SFCHECK: A unified set of procedures for evaluating the quality of macromolecular structure-factor data and their agreement with the atomic model. *Acta Crystallogr. D55*, 191–205.
2. Blankenship, R. E. (2002) Antenna complexes and energy transfer processes. In *Molecular mechanisms of photosynthesis* (Blankenship, R. E., Ed.) 2nd ed., pp 61−94. Blackwell Science, Oxford, U.K.
3. Macpherson, A. N., and Hiller, R. G. (2003) Light-harvesting systems in chlorophyll c-containing algae. In *Advances in photosynthesis and respiration. Volume 13: Light harvesting antennas* (Green, B. R., and Parson, W. W., Eds.) 1st ed., pp 323−352, Kluwer Academic Publishers, Dordrecht, The Netherlands.
4. Mimuro, M., and Kikuchi, H. (2003) Antenna systems and energy transfer in cyanophyta and rhodophyta. In *Advances in photosynthesis and respiration. Volume 13: Light harvesting antennas* (Green, B. R., and Parson, W. W., Eds.) 1st ed., pp 282−306, Kluwer Academic Publishers, Dordrecht, The Netherlands.
5. Polívka, T., and Sundström, V. (2004) Ultrafast dynamics of carotenoid excited states: From solution to natural and artificial systems. *Chem. Rev. 104*, 2021–2071.
6. Christensen, R. L. (1999) The Electronic States of Carotenoids. In *The Photochemistry of Carotenoids* (Frank, H. A., Young, A. J., Britton, G., and Cogdell, R. J., Eds.) pp 137−157, Kluwer Academic Publishers, Dordrecht, The Netherlands.
7. Polívka, T., Hiller, R. G., and Frank, H. A. (2007) Spectroscopy of the peridinin-chlorophyll-a protein: Insight into light-harvesting strategy of marine algae. *Arch. Biochem. Biophys. 458*, 111–120.
8. Bautista, J. A., Connors, R. E., Raju, B. B., Hiller, R. G., Sharples, F. P., Gosztola, D., Wasielewski, M. R., and Frank, H. A. (1999) Excited State Properties of Peridinin: Observation of a Solvent Dependence of the Lowest Excited Singlet State Lifetime and Spectral Behavior Unique among Carotenoids. *J. Phys. Chem. B 103*, 8751–8758.
9. Frank, H. A., Bautista, J. A., Josue, J., Pendon, Z., Hiller, R. G., Sharples, F. P., Gosztola, D., and Wasielewski, M. R. (2000) Effect of the Solvent Environment on the Spectroscopic Properties and Dynamics of the Lowest Excited States of Carotenoids. *J. Phys. Chem. B 104*, 4569–4577.
10. Zigmantas, D., Polivka, T., Hiller, R. G., Yartsev, A., and Sundstrom, V. (2001) Spectroscopic and Dynamic Properties of the Peridinin Lowest Singlet Excited States. *J. Phys. Chem. A 105*, 10296–10306.
11. Zigmantas, D., Hiller, R. G., Sharples, F. P., Frank, H. A., Sundstrom, V., and Polivka, T. (2004) Effect of a conjugated carbonyl group on the photophysical properties of carotenoids. *Phys. Chem. Chem. Phys. 6*, 3009–3016.
12. Zigmantas, D., Hiller, R. G., Sundstrom, V., and Polivka, T. (2002) Carotenoid to chlorophyll energy transfer in the peridinin-chlorophyll-a-protein complex involves an intramolecular charge transfer state. *Proc. Natl. Acad. Sci. U.S.A. 99*, 16760–16765.
13. Hofmann, E., Wrench, P. M., Sharples, F. P., Hiller, R. G., Welte, W., and Diederichs, K. (1996) Structural basis of light harvesting by carotenoids: Peridinin-chlorophyll-protein from *Amphidinium carterae*. *Science 272*, 1788–1791.
14. Hiller, R. G., Crossley, L. G., Wrench, P. M., Santucci, N., and Hofmann, E. (2001) The 15-kDa forms of the apo-peridinin-chlorophyll a protein (PCP) in dinoflagellates show high identity with the apo-32 kDa PCP forms, and have similar N-terminal leaders and gene arrangements. *Mol. Genet. Genomics 266*, 254–259.
15. Weis, V., Verde, E., and Reynolds, W. (2002) Characterization of a short form Peridinin-Chlorophyll a-Protein (PCP) from the symbiotic dinoflagellate *Symbodinium muscatinei* (Dinophycae) from the sea anemone *Anthopleura elegantissima* (Cnidaria). *J. Phycol. 38*, 157–163.
16. Prézelin, B. B., and Haxo, F. T. (1976) Purification and characterization of peridinin-chlorophyll a-proteins from the marine dinoflagellates *Glenodinium* sp. and *Gonyaulax polyedra*. *Planta 128* 133–141.
17. Carbonera, D., Giacometti, G., Segre, U., Hofmann, E., and Hiller, R. G. (1999) Structure-Based Calculations of the Optical Spectra of the Light-Harvesting Peridinin-Chlorophyll-Protein Complexes from *Amphidinium carterae* and *Heterocapsa pygmaea*. *J. Phys. Chem. B 103*, 6349–6356.
18. Damjanović, A., Ritz, T., and Schulten, K. (2000) Excitation transfer in the peridinin-chlorophyll-protein of *Amphidinium carterae*. *Biophys. J. 79*, 1695–1705.
19. Kleima, F. J., Hofmann, E., Gobets, B., van Stokkum, I. H., van Grondelle, R., Diederichs, K., and van Amerongen, H. (2000) Förster excitation energy transfer in peridinin-chlorophyll-a-protein. *Biophys. J. 78*, 344–353.
20. Ilagan, R. P., Shima, S., Melkozernov, A., Lin, S., Blankenship, R. E., Sharples, F. P., Hiller, R. G., Birge, R. R., and Frank, H. A. (2004) Spectroscopic properties of the main-form and high-salt peridinin-chlorophyll a proteins from *Amphidinium carterae*. *Biochemistry 43*, 1478–1487.
21. Polívka, T., Pascher, T., Sundström, V., and Hiller, R. G. (2005) Tuning energy transfer in the peridinin-chlorophyll complex by reconstitution with different chlorophylls. *Photosynth. Res. 86*, 217–227.
22. Polívka, T., Pascher, T., and Hiller, R. G. (2008) Energy transfer in the peridinin-chlorophyll protein complex reconstituted with mixed chlorophyll sites. *Biophys. J. 94*, 3198–3207.
23. Mackowski, S., Wörmke, S., Brotosudarmo, T. H. P., Jung, C., Hiller, R. G., Scheer, H., and Bräuchle, C. (2007) Energy transfer in reconstituted peridinin-chlorophyll-protein complexes: Ensemble and single-molecule spectroscopy studies. *Biophys. J. 93*, 3249–3258.
24. Krueger, B. P., Lampoura, S. S., van Stokkum, I. H., Papagiannakis, E., Salverda, J. M., Gradinaru, C. C., Rutkauskas, D., Hiller, R. G., and van Grondelle, R. (2001) Energy transfer in the peridinin chlorophyll-a protein of *Amphidinium carterae* studied by polarized transient absorption and target analysis. *Biophys. J. 80*, 2843–2855.
25. Linden, P. A., Zimmermann, J., Brixner, T., Holt, N. E., Vaswani, H. M., Hiller, R. G., and Fleming, G. R. (2004) Transient Absorption Study of Peridinin and Peridinin-Chlorophyll a-Protein after Two-Photon Excitation. *J. Phys. Chem. B 108*, 10340–10345.
26. Akimoto, S., Takaichi, S., Ogata, T., Nishimura, Y., Yamazaki, I., and Mimuro, M. (1996) Excitation energy transfer in carotenoid-chlorophyll protein complexes probed by femtosecond fluorescence decays. *Chem. Phys. Lett. 260*, 147–152.
27. Bautista, J. A., Hiller, R. G., Sharples, F. P., Gosztola, D., Wasielewski, M., and Frank, H. A. (1999) Singlet and Triplet Energy Transfer in the Peridinin-Chlorophyll a-Protein from *Amphidinium carterae*. *J. Phys. Chem. A 103*, 2267–2273.
28. Shima, S., Ilagan, R. P., Gillespie, N., Sommer, B. J., Hiller, R. G., Sharples, F. P., Frank, H. A., and Birge, R. R. (2003) Two-Photon and Fluorescence Spectroscopy and the Effect of Environment on the Photochemical Properties of Peridinin in Solution and in the Peridinin-Chlorophyll-Protein from *Amphidinium carterae*. *J. Phys. Chem. A 107*, 8052–8066.
29. Sharples, F. P., Wrench, P. M., Ou, K., and Hiller, R. G. (1996) Two distinct forms of the peridinin-chlorophyll a-protein from *Amphidinium carterae*. *Biochim. Biophys. Acta 1276*, 117–123.
30. Ilagan, R. P., Koscielecki, J. F., Hiller, R. G., Sharples, F. P., Gibson, G. N., Birge, R. R., and Frank, H. A. (2006) Femtosecond time-resolved absorption spectroscopy of main-form and high-salt peridinin-chlorophyll a-proteins at low temperatures. *Biochemistry 45*, 14052–14063.
31. Kabsch, W. (1993) Automatic processing of rotation diffraction data from crystals of initially unknown symmetry and cell constants. *J. Appl. Crystallogr. 26*, 795–800.
32. Vagin, A., and Teplyakov, A. (1997) MOLREP: An Automated Program for Molecular Replacement. *J. Appl. Crystallogr. 30*, 1022–1025.
33. Collaborative Computational Project No. 4 (1994) The CCP4 suite: Programs for protein crystallography. *Acta Crystallogr. D50*, 760–763.
34. Brünger, A. T., Adams, P. D., Clore, G. M., DeLano, W. L., Gros, P., Grosse-Kunstleve, R. W., Jiang, J. S., Kuszewski, J., Nilges, M., Pannu, N. S., Read, R. J., Rice, L. M., Simonson, T., and Warren, G. L. (1998) Crystallography & NMR system: A new software suite for macromolecular structure determination. *Acta Crystallogr. D54*, 905–921.
35. Emsley, P., and Cowtan, K. (2004) Coot: Model-building tools for molecular graphics. *Acta Crystallogr. D60*, 2126–2132.
36. Terwilliger, T. C. (2000) Maximum-likelihood density modification. *Acta Crystallogr. D56*, 965–972.

37. Schüttelkopf, A. W., and van Aalten, D. M. F. (2004) PRODRG: A tool for high-throughput crystallography of protein-ligand complexes. *Acta Crystallogr. D60*, 1355–1363.
38. Kleywegt, G. J., and Jones, T. A. (1997) Model building and refinement practice. *Methods Enzymol. 277*, 208–230.
39. Vriend, G. (1990) WHAT IF: A molecular modeling and drug design program. *J. Mol. Graphics 8*, 52–56, 29.
40. DeLano, W. L. (2002) *The PyMOL User's Manual*, DeLano Scientific, Palo Alto, CA.
41. Krissinel, E., and Henrick, K. (2004) Secondary-structure matching (SSM), a new tool for fast protein structure alignment in three dimensions. *Acta Crystallogr. D60*, 2256–2268.
42. Di Valentin, M., Ceola, S., Salvadori, E., Agostini, G., Giacometti, G. M., and Carbonera, D. (2008) Spectroscopic properties of the peridinins involved in chlorophyll triplet quenching in high-salt peridinin-chlorophyll a-protein from *Amphidinium carterae* as revealed by optically detected magnetic resonance, pulse EPR and pulse ENDOR spectroscopies. *Biochim. Biophys. Acta 1777*, 1355–1363.
43. Kleywegt, G. J., and Jones, T. A. (1994) A super position *CCP4/ESF-EACBM Newsletter on Protein Crystallography 31*, 9–14.
44. Müh, F., Madjet, M. E., Adolphs, J., Abdurahman, A., Rabenstein, B., Ishikita, H., Knapp, E., and Renger, T. (2007) α-Helices direct excitation energy flow in the Fenna Matthews Olson protein. *Proc. Natl. Acad. Sci. U.S.A. 104*, 16862–16867.
45. Förster, T. (1948) Zwischenmolekulare Energiewanderung und Fluoreszenz. *Ann. Phys. 437*, 55–75.
46. Durbeej, B., and Eriksson, L. A. (2006) Protein-bound chromophores astaxanthin and phytochromobilin: Excited state quantum chemical studies. *Phys. Chem. Chem. Phys. 8*, 4053–4071.
47. Linnanto, J., and Korppi-Tommola, J. (2006) Quantum chemical simulation of excited states of chlorophylls, bacteriochlorophylls and their complexes. *Phys. Chem. Chem. Phys. 8*, 663–687.
48. Robert, B., Cogdell, R., and van Grondelle, R. (2003) The light harvesting system of purple bacteria. In *Advances in photosynthesis and respiration. Volume 13: Light harvesting antennas* (Green, B., and Parson, W., Eds.) 1st ed., pp 169−194, Kluwer Academic Publishers, Dordrecht, The Netherlands.
49. Cogdell, R. J., Gall, A., and Köhler, J. (2006) The architecture and function of the light-harvesting apparatus of purple bacteria: From single molecules to in vivo membranes. *Q. Rev. Biophys. 39*, 227–324.
50. Di Valentin, M., Ceola, S., Salvadori, E., Agostini, G., and Carbonera, D. (2008) Identification by time-resolved EPR of the peridinins directly involved in chlorophyll triplet quenching in the peridinin-chlorophyll a-protein from *Amphidinium carterae*. *Biochim. Biophys. Acta 1777*, 186–195.
51. Di Valentin, M., Ceola, S., Agostini, G., Giacometti, G. M., Angerhofer, A., Crescenzi, O., Barone, V., and Carbonera, D. (2008) Pulse ENDOR and density functional theory on the peridinin triplet state involved in the photo-protective mechanism in the peridinin-chlorophyll a-protein from *Amphidinium carterae*. *Biochim. Biophys. Acta 1777*, 295–307.
52. Alexandre, M. T. A., Luhrs, D. C., van Stokkum, I. H. M., Hiller, R., Groot, M., Kennis, J. T. M., and van Grondelle, R. (2007) Triplet State Dynamics in Peridinin-Chlorophyll-a-Protein: A New Pathway of Photoprotection in LHCs?. *Biophys. J. 93*, 2118–2128.
53. Stokkum, I. H. V., Papagiannakis, E., Vengris, M., Salverda, J. M., Polivka, T., Zigmantas, D., Larsen, D. S., Lampoura, S. S. Hiller, R. G., and Grondelle, R. V. (2009) Inter-pigment interactions in the peridinin chlorophyll protein studied by global and target analysis of time resolved absorption spectra. *Chem. Phys. 357* 70–78.
54. Zucchelli, G., Brogioli, D., Casazza, A. P., Garlaschi, F. M., and Jennings, R. C. (2007) Chlorophyll ring deformation modulates Qy electronic energy in chlorophyll-protein complexes and generates spectral forms. *Biophys. J. 93*, 2240–2254.
55. Shelnutt, J. A., Song, X., Ma, J., Jia, S., Jentzen, W., Medforth, C. J., and Medforth, C. J. (1998) Nonplanar porphyrins and their significance in proteins. *Chem. Soc. Rev. 27*, 31–42.
56. Papagiannakis, E., Vengris, M., Larsen, D. S., van Stokkum, I. H. M., Hiller, R. G., and van Grondelle, R. (2006) Use of ultrafast dispersed pump-dump-probe and pump-repump-probe spectroscopies to explore the light-induced dynamics of peridinin in solution. *J. Phys. Chem. B 110*, 512–521.
57. Bas, D. C., Rogers, D. M., and Jensen, J. H. (2008) Very fast prediction and rationalization of pKa values for protein-ligand complexes. *Proteins 73*, 765–783.
58. Petrek, M., Otyepka, M., Banás, P., Kosinová, P., Koca, J., and Damborský, J. (2006) CAVER: A new tool to explore routes from protein clefts, pockets and cavities. *BMC Bioinf. 7*, 316.
59. Miller, D. J., Catmull, J., Puskeiler, R., Tweedale, H., Sharples, F. P., and Hiller, R. G. (2005) Reconstitution of the peridinin-chlorophyll a protein (PCP): Evidence for functional flexibility in chlorophyll binding. *Photosynth. Res. 86*, 229–240.
60. Zigmantas, D., Hiller, R. G., Yartsev, A., Sundstrom, V., and Polivka, T. (2003) Dynamics of Excited States of the Carotenoid Peridinin in Polar Solvents: Dependence on Excitation Wavelength, Viscosity, and Temperature. *J. Phys. Chem. B 107*, 5339–5348.
61. Liaaen-Jensen, S., and Kildahl-Andersen, G. (2008) Blue carotenoids. *ARKIVOC (Gainesville, FL, U.S.) 4*, 5–25.
62. Ren, L., Martin, C. H., Wise, K. J., Gillespie, N. B., Luecke, H., Lanyi, J. K., Spudich, J. L., and Birge, R. R. (2001) Molecular mechanism of spectral tuning in sensory rhodopsin II. *Biochemistry 40*, 13906–13914.
63. Kochendoerfer, G. G., Wang, Z., Oprian, D. D., and Mathies, R. A. (1997) Resonance Raman examination of the wavelength regulation mechanism in human visual pigments. *Biochemistry 36* 6577–6587.
64. Davis, I. W., Leaver-Fay, A., Chen, V. B., Block, J. N., Kapral, G. J., Wang, X., Murray, L. W., Arendall, W. B., Snoeyink, J., Richardson, J. S., and Richardson, D. C. (2007) MolProbity: All-atom contacts and structure validation for proteins and nucleic acids. *Nucleic Acids Res. 35*, W375–W383.
65. Pettersen, E. F., Goddard, T. D., Huang, C. C., Couch, G. S., Greenblatt, D. M., Meng, E. C., and Ferrin, T. E. (2004) UCSF Chimera: A visualization system for exploratory research and analysis. *J. Comput. Chem. 25*, 1605–1612.